© 2015. Published by The Company of Biologists Ltd | The Journal of Experimental Biology (2015) 218, 2518-2527 doi:10.1242/jeb.116228

RESEARCH ARTICLE

Kinematics and aerodynamics of avian upstrokes during slow flight

Kristen E. Crandell* and Bret W. Tobalske

ABSTRACT

Slow flight is extremely energetically costly per unit time, yet highly important for takeoff and survival. However, at slow speeds it is presently thought that most birds do not produce beneficial aerodynamic forces during the entire wingbeat: instead they fold or flex their wings during upstroke, prompting the long-standing prediction that the upstroke produces trivial forces. There is increasing evidence that the upstroke contributes to force production, but the aerodynamic and kinematic mechanisms remain unknown. Here, we examined the wingbeat cycle of two species: the diamond dove (*Geopelia cuneata*) and zebra finch (*Taeniopygia guttata*), which exhibit different upstroke styles – a wingtip-reversal and flexed-wing upstroke, respectively. We used a combination of particle image velocimetry and near-wake streamline measures alongside detailed 3D kinematics. We show that during the middle of the wingtip-reversal upstroke, the hand-wing has a high angular velocity (15.3±0.8 deg ms^{-1}) and translational speed (8.4±0.6 m s^{-1}). The flexed-wing upstroke, in contrast, has low wingtip speed during mid-upstroke. Instead, later in the stroke cycle, during the transition from upstroke to downstroke, it exhibits higher angular velocities (45.5±13.8 deg ms^{-1}) and translational speeds (11.0±1.9 m s^{-1}). Aerodynamically, the wingtip-reversal upstroke imparts momentum to the wake, with entrained air shed backward (visible as circulation of 14.4±0.09 m^2 s^{-1}). In contrast, the flexed-wing upstroke imparts minimal momentum. Clap and peel in the dove enhances the time course for circulation production on the wings, and provides new evidence of convergent evolution on time-varying aerodynamic mechanisms during flapping in insects and birds.

KEY WORDS: Lift, Thrust, Clap and peel, Take-off, Wingtip-reversal, Flexed-wing, Particle image velocimetry

INTRODUCTION

Takeoff, landing and slow flight are critical phases for all flying animals, whether foraging, evading predation or finding a mate. Slow flight (<3 m s^{-1}) is also an energetically costly form of flight (Tobalske et al., 2003). The aerodynamics of this important form of flight are not well understood because the majority of research on bird flight aerodynamics has focused either on hovering in hummingbirds (Warrick et al., 2005, 2009) or on medium- and high-speed flight (Spedding et al., 2003a,b; Spedding and Hedenstrom, 2009; Henningsson et al., 2011; Spedding and Hedenstrom, 2009). Here, we set out to test the hypothesis that there is aerodynamic activity during the general avian (i.e. non-hummingbird) upstroke, an idea proposed first by Marey (1890) and subsequently by Lorenz (1933) and Brown (1953). We describe the kinematic and aerodynamic patterns of slow flight in two species of birds, the diamond dove and the zebra finch, with two distinct upstroke styles: wingtip-reversal and flexed-wing upstroke.

When engaged in slow flight, birds generally do not maintain an extended wing. Instead, all birds except hummingbirds (Warrick et al., 2005) fold or flex their wings on the upstroke (Tobalske, 2007). During medium and fast flight in many species, the wing is kept partially extended during upstroke, and so is understood to be aerodynamically active (Spedding et al., 2003b), particularly at faster speeds (Henningsson et al., 2011). In contrast, the observed kinematic patterns during slow flight have prompted the well-established prediction that the upstroke is aerodynamically inactive, halving the amount of time during a wingbeat that a bird can produce useful forces. Few direct measures of the kinematics and aerodynamics of upstroke in slow flight exist, however (Chang et al., 2013; Hedenström et al., 2006; Lentink et al., 2015; Muijres et al., 2012a,b,c; Spedding et al., 2003a). Most studies of takeoff flight focus on the immediate transition from legs to wings (Berg and Biewener, 2010; Earls, 2000; Provini et al., 2012).

During slow flight, most birds have one of two upstroke patterns: a flexed-wing upstroke or a wingtip-reversal upstroke. During the flexed-wing upstroke, the entire wing is pulled toward the body. Birds with this pattern generally have low aspect ratio, rounded wing tips (Brown, 1963). A study of slow flight in flycatchers (*Ficedula hypoleuca*) found no evidence for an aerodynamically active flexed-wing upstroke (Muijres et al., 2012a). The flexed-wing upstroke becomes aerodynamically active gradually as flight speed increases from 4 m s^{-1} to 8 m s^{-1} in both the thrush nightingale (Spedding et al., 2003b) and the robin (Hedenström et al., 2006), yet aerodynamic activity at speeds less than 4 m s^{-1} remains untested. The contrasting wingtip-reversal upstroke style keeps the distal wing extended, with the primary feathers supinated but traveling through an arc in the air. Birds with pointed, high aspect-ratio wingtips tend to exhibit a tip-reversal upstroke during slow flight (Simpson, 1983; Tobalske, 2007); galliformes are an exception (Tobalske and Dial, 2000).

Several lines of evidence suggest the tip-reversal upstroke produces aerodynamic force. Feather loading in live pigeons (*Columba livia*) and propeller models using pigeon wings suggest that the tip-reversal upstroke is aerodynamically active (Corning and Biewener, 1998; Crandell and Tobalske, 2011). *In vivo* accelerometers mounted to the trunk of a cockatiel (*Nymphicus hollandicus*) also indicate that the tip-reversal upstroke produces 14% of the net force of downstroke (Hedrick et al., 2004). Lastly, kinematic analyses of pigeons suggest the upstroke produces 50% of the net force of the downstroke during slow-speed maneuvering (Ros et al., 2011). However, the aerodynamic mechanism remains unknown.

It has been hypothesized, based on wing kinematics (Bennett, 1977; Scholey, 1983; Simpson, 1983), that birds which produce a tip-reversal upstroke capitalize on a time-varying mechanism called clap and fling (or clap and peel). This mechanism creates circulation at the transition from upstroke to downstroke via an interaction

Field Research Station at Fort Missoula, Division of Biological Sciences, University of Montana, Missoula, MT 59812, USA.

*Author for correspondence (kristen.crandell@gmail.com)

Received 2 November 2014; Accepted 25 May 2015

The Journal of Experimental Biology

The Journal of Experimental Biology (2015) 218, 2518-2527 doi:10.1242/jeb.116228

List of symbols and abbreviations

A	area swept by the wing
c	wing chord
F	net force
PIV	particle image velocimetry
T	time interval
u	average airspeed
V_A	angular velocity
V_T	global wingtip speed
α	global angle of attack
β	angle between wings
Γ	circulation
ρ	air density
ω	vorticity

Table 1. Morphometrics for individual birds

	Mass (g)	Wing area (cm^2)	Wing length (cm)	Wing chord (cm)	Aspect ratio
Dove					
2	43.3	46.81	10.56	5.79	0.99
3	38.7	38.67	9.65	4.99	1.10
4	40.3	60.14	11.54	5.62	0.83
5	38.2	75.45	11.83	6.59	0.68
Mean±s.d.	40.1±2.3	55.3±16.1	10.9±1.0	5.7±0.6	0.9±0.2
Finch					
1	13	29.41	6.92	4.69	1.08
2	12.2	28.7	6.62	5.8	1.06
3	12.1	36.79	8.44	5.32	1.03
4	12.5	29.88	8.04	4.59	1.21
Mean±s.d.	12.5±0.4	7.5±0.9	5.1±0.6	5.1±0.6	1.1±0.1

All birds were used in particle image velocimetry (PIV) and kinematic analyses. Dove 4 and finch 1 were used in smoke-line flow studies.

between the left and right wings. Similar insect kinematic patterns were first observed in *Drosophila melanogaster* and described by Vogel (1967). Weis-Fogh described this pattern in the chalcid wasp *Encarsia formosa* and predicted this motion increases the strength of circulation around the wing (Weis-Fogh, 1973). Subsequent models indicated the fling is aerodynamically active (Maxworthy, 1979) by initiating circulation immediately along the wing. This circulation contributes heavily to a leading-edge vortex that grows throughout the downstroke (Sane, 2003). Clap and fling is observed in a large insect, the hawkmoth (*Re*=8000) (Bomphrey et al., 2006). Theory and empirical measurements with flapper models both indicate a boost in force production via this mechanism (Ellington, 1984; Lehmann et al., 2005). Among birds, there exists aerodynamic evidence that Japanese white-eye (*Zosterops japonicus*) and Gouldian finch (*Erythrura gouldiae*) capitalize on a ventral clap, wherein the wings are brought together beneath the body to contribute to the downwash (Chang et al., 2013). Here, we differentiate between a clap and fling versus a clap and peel, as defined by Miller and Peskin (2009): we define a clap and fling as minimal flexibility in a rigid wing structure, wherein changes in shape are from external mechanisms, such as aerodynamic loading and inertia; clap and peel, then, has flexibility spanwise and chordwise along the wing, and shape changes are both passive and active via musculoskeletal control.

We undertook the present study to test for aerodynamic activity in both upstroke styles, and describe the kinematics in relation to the forces they produce. We tested the following hypotheses: the kinematic clap and peel pattern yields flow regimes similar to the clap and peel of insect flight, despite dramatic differences in body size and, thus, Reynolds number (hawkmoth *Re*=8000, dove *Re*=51,000). Additionally, the flexed-wing upstroke will be aerodynamically inactive. In both birds, we additionally expected the aerodynamic circulation (or lack thereof) produced during the upstroke would carry over and impact the circulation produced during the downstroke. To address these hypotheses, we compared two species: the diamond dove [*Geopelia cuneata* (Latham 1801), 40 g], which exhibits a wingtip-reversal upstroke, and the zebra finch (*Taeniopygia guttata* Reichenbach 1862, 13 g), which uses a flexed-wing upstroke.

RESULTS

Kinematics

We analyzed kinematic patterns for the third wingbeat in a flight sequence for four birds of both species (morphometrics available in Table 1). All flights were within ±5 deg of level flight. In kinematic trials, the doves had an average body velocity of 1.54±0.36 m s^{-1}, while the finches had an average body velocity of 1.03±0.28 m s^{-1}. During the third wingbeat, the doves were still accelerating at an average of 5.5±0.54 m s^{-2}, and finches were accelerating at 4.34±1.54 m s^{-2}.

Three-dimensional traces of the path of the wingtips of the dove and finch followed the general pattern of the lateral-view kinematics of the rock pigeon and black-billed magpie (*Pica hudsonia*), respectively, as described in Tobalske and Dial (1996). Our 3D analysis revealed a figure-of-eight pattern in the dorsal and sagittal plane of the dove, but not in the finch (Fig. 1). The finch pattern produced a near-complete semi-circle in both the dorsal and sagittal planes, where the wingtip (black line) was kept caudal to the body during the upstroke, and oriented cranially during downstroke. In the dove, the wingtip transitioned from cranial to caudal during the upstroke (Fig. 1, dorsal and sagittal planes). A further difference between the species was visible in the transverse plane. In the dove, the hand-wing was kept extended (80.2±3.2% of wing length) during both upstroke and downstroke. In contrast, the finch flexed the wing (64.8±5.2% of wing length) during upstroke, most noticeably in the wrist kinematics (Fig. 1, transverse plane).

The global angle of attack (α, defined as the angle between the velocity vector of the hand-wing and the wrist–secondary feather chord line) differed between species during upstroke, but followed a similar trend (Fig. 2A). The dove had a negative α during upstroke, with a minimum of −81.3±4 deg during the first third of upstroke. The dove transitioned from a negative to a positive α at wing turn around. In the finch, during upstroke, α remained negative, with a minimum value of −45.9±7.3 deg. As the transition between upstroke and downstroke approached, α transitioned through 0 deg, peaking during the downstroke at 51.5±7.4 deg.

Global wingtip speed (V_T) showed similar patterns between the dove and finch (Fig. 2B). In the dove, there were two peaks in V_T, the first during upstroke at 8.4±0.6 m s^{-1}, and the second during downstroke at 9.9±1.3 m s^{-1}. These indicate maximal V_T produced during the middle of the limb swing phase, at the transition from limb acceleration to limb deceleration. The finch also exhibited two peaks, although the peak during upstroke remained for approximately 5 ms. During the upstroke, peak V_T was 7.5±3.3 m s^{-1}. During the downstroke, V_T peaked at 11.0±1.9 m s^{-1}. This peak occurred following the transition from upstroke to downstroke, and so took place relatively earlier in the finch than the dove.

Angular velocities (V_A) were defined as the angular change between the orientation of the position vector of the hand-wing

The Journal of Experimental Biology (2015) 218, 2518-2527 doi:10.1242/jeb.116228

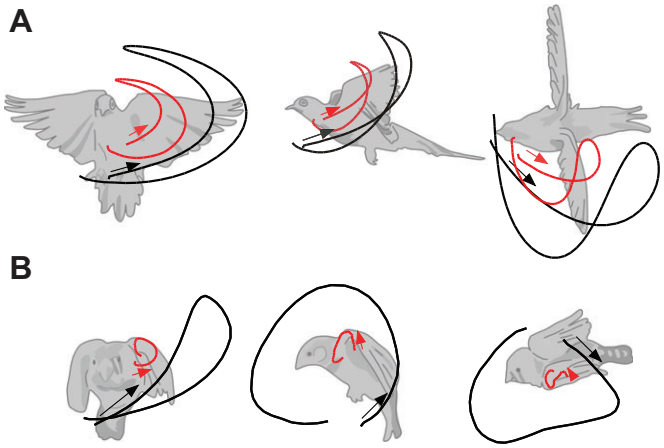

Fig. 1. Traces of representative bird-centered wingtip and wrist movements of the study species. (A) Diamond dove, (B) zebra finch. Traces (left to right) are from the transverse, sagittal and dorsal planes (bird silhouettes represent the mid-upstroke position, and are not an exact representation of posture at that point in time). Wrists are represented in red, wingtips in black. Arrows indicate the start of upstroke (transition from downstroke, time 0%).

centroid points, in global coordinates. These velocities followed a similar pattern to wingtip speed in the dove, but not the finch (Fig. 2C). In the dove, two peaks in V_A occurred, in the same pattern as V_T – peaking halfway through upstroke at 15.3±0.8 deg ms^{-1} and halfway through downstroke at 19.4±2.1 deg ms^{-1}. In the finch, however, only one prominent peak in V_A occurred, at 45.4± 13.8 deg ms^{-1}, at the transition between upstroke and downstroke. At this point, the wing rapidly reoriented from being strongly adducted to being fully extended. A minor V_A peak occurred during the upstroke at 32.2±9.7 deg ms^{-1}, but this peak remained relatively stable until the transition between upstroke and downstroke.

Our analysis of wing–wing interactions in three dimensions illustrates each portion of the clap and peel cycle in the dove, relative to wing contact time (Fig. 3). In the wingtip-reversal at the end of the upstroke, the rapidly extending wings came into contact (the 'clap'), with the left and right wing leading edges coming together approximately 3 ms before the trailing edge, at approximately 5% of the entire wingbeat cycle. The wingtip leading edges were 1.5±0.6 cm apart (approximately the width between the shoulders) at closest contact, while the trailing edges reached almost full contact at 0.2±0.1 cm apart. Fig. 3A illustrates the leading edge (red, orange) on the right and left wing coming into contact (red arrow). The trailing edge (Fig. 3A, blue, green) came together later (blue arrow). Following the clap, the wings moved apart during the peel phase as downstroke began. The wings first separated at the leading edge (Fig. 3A, red arrow), with the trailing edge separation occurring 4–9 ms later (blue and green arrows).

In contrast, during the flexed-wing upstroke of the zebra finch, all points along the wing stayed close to the body during upstroke, with the wingtip at 3.2±0.4 cm between the left and right wings (approximately the width of the body, Fig. 3B). At the transition from upstroke to downstroke, the wings opened approximately 6.2±0.7 cm apart. Notably, the trailing edges of the finch did come close to contact during the transition from upstroke to downstroke (Fig. 3B, blue and green).

Aerodynamics

We analyzed the wake of four birds for each species (morphometrics available in Table 1). Zebra finches averaged a body velocity of

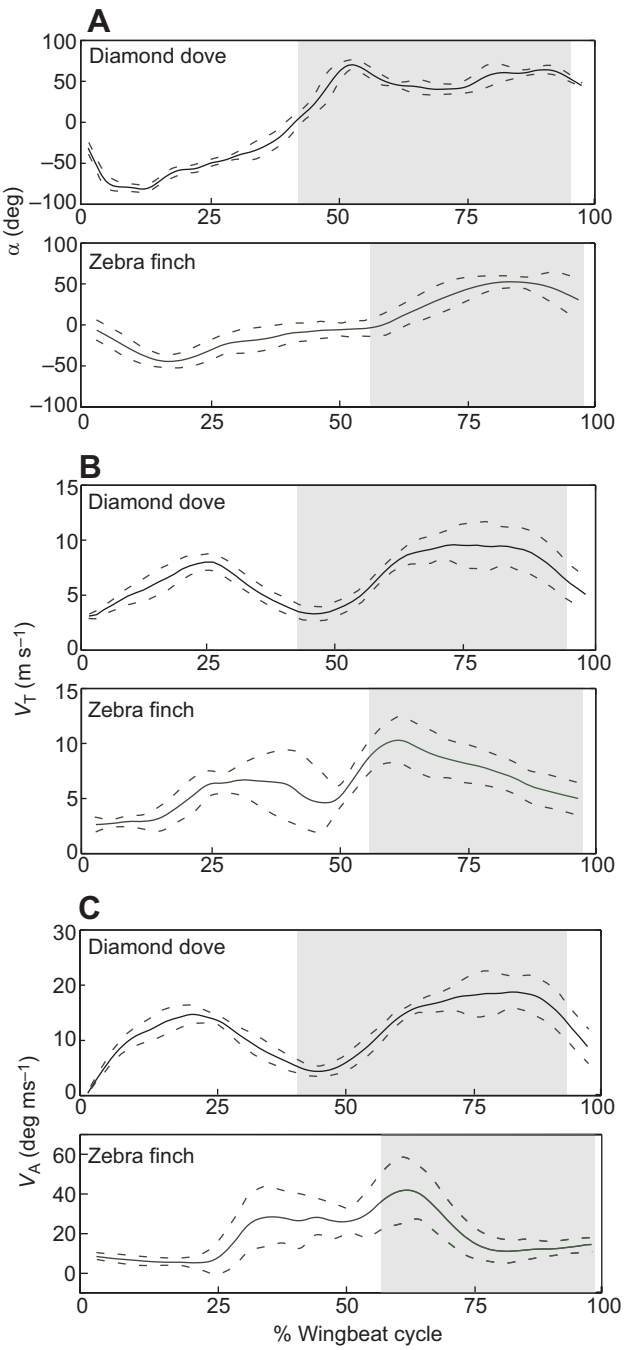

Fig. 2. Kinematic variables for the centroid of the hand-wing. (A) Angle of attack (α), (B) translational speed (wingtip speed, V_T) and (C) angular velocity (V_A). Data were extracted from the diamond dove and zebra finch during the third wingbeat of the downstroke. Solid lines represent means, dashed lines the standard deviations. The shaded area represents the downstroke.

1.03±0.28 m s^{-1} and diamond doves averaged a body velocity of 1.54±0.36 m s^{-1}; both species were accelerating. Flights analyzed with smoke visualization maintained free-stream velocities of approximately 0.95±0.05 m s^{-1}. All flights analyzed were within ±5 deg of level flight. We observed significant aerodynamic activity in the wingtip-reversal upstroke of the diamond dove, and minimal activity during the flexed-wing upstroke of the zebra finch. In the dove, a shed vortex was evident in our particle image velocimetry (PIV) images (Fig. 4) at the transition from upstroke to downstroke (circulation Γ=14.4±0.09 m s^{-2}). This same type of

The Journal of Experimental Biology (2015) 218, 2518-2527 doi:10.1242/jeb.116228

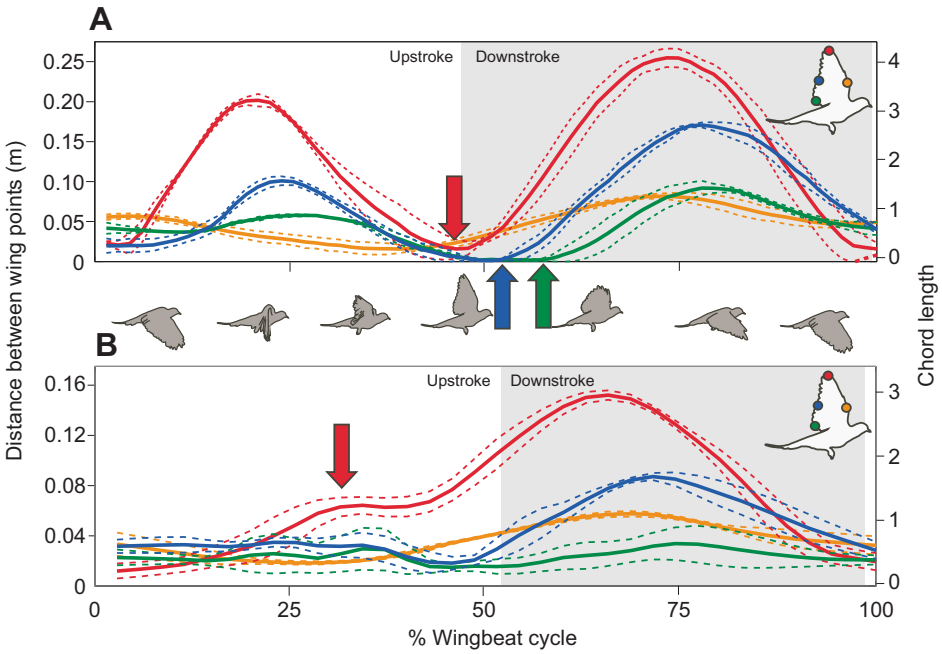

Fig. 3. Distances between opposite wings during the third full wingbeat cycle in diamond doves and zebra finches. (A) Distance between wing points in the diamond dove. Note the significant lag time between leading edge separation (red, orange) and trailing edge separation (blue, green). Arrows show contact and separation of wingtips (red) before trailing edges (blue, green). (B) Distance between wing points in the zebra finch. Note the distinct kinematic differences from the dove during upstroke, as the finch holds its wings close to the body during this phase (orange, blue, green). The leading edge wingtip (red) is held close to the body during the start of upstroke in the finch, and these edges begin to separate over 2/3 of the way through the upstroke time (red arrow). Means and s.e. are represented by solid and dashed lines, respectively. The scale on the right is relative to the wing chord (Table 1). Bird outlines between graphs are modeled after the diamond dove.

upstroke-generated vortex was never observed in PIV images from the zebra finch (Fig. 5).

During the last half of upstroke, the diamond dove hand-wing was aerodynamically active in that it displaced streamlines (Fig. 6A). Induced velocity to the air was visible as an abrupt cut-off between the smoke lines through which the wing moved, visible at 35% and 45% of the wingbeat cycle in Fig. 6A (red arrowhead and ellipse). At the end of upstroke (Fig. 6A, 55%), the wings came into contact, and the entrained air around the wings was shed. As described above, we detected this shed vortex in our parasagittal samples of PIV images as circulation deposited into the wake at the transition between upstroke and downstroke in the diamond dove (Fig. 4A). Induced velocity behind the wing was also visible, at 2.73±0.23 ms^{-1} for an arbitrarily selected patch immediately behind the wings (Fig. 7).

From smoke lines near the finch, it was evident that the feathers act similar to those in the doves, imparting momentum to the wake; smoke was entrained on the primary feathers during upstroke (Fig. 6B, 10 ms, red arrowhead; supplementary material Movie 1). However, the surface area of the wing was much reduced in comparison to the dove (Fig. 6).

Both species created a starting vortex during the first part of downstroke (Fig. 4B and Fig. 5B), but the initiation of circulation appeared to be relatively earlier in the dove (Fig. 4A), which we interpret as being due to the clap and peel pattern of the wings, approximately concurrent with the shedding of circulation into the wake. We first measured this circulation in a parasagittal plane over the back of the bird as 26±3% the value of the final downstroke circulation (Fig. 8). In the dove, this circulation grew throughout the downstroke (Fig. 4), and reached values that were not significantly different from the final shed vortex halfway through the downstroke. In contrast, circulation measured in the zebra finch in the same plane was approximately 0% of final circulation values at the start of early downstroke (Fig. 5A and Fig. 8). This was a consequence of the lack of an initial shed vortex created during upstroke. However, as observed in the smoke line video, the finch had a start vortex that began independently on both wings, just like the dove (supplementary material Movie 1). As a consequence of this right and left wing-independent vortex ring structure (Pournazeri et al., 2013), the measured circulation in the sagittal plane dorsal to the bird was 20–40% lower in the finch at the start of downstroke, suggesting a relatively smaller time interval over which circulation was created. This smaller time frame was a consequence of the wings of the finch beginning the downstroke farther from the midline of the bird (Fig. 3).

Force estimates in the dove

To provide a rough estimate of the net forces that the clap and peel mechanism may provide relative to the subsequent downstroke, we adopted two models: a momentum-jet model (Vogel, 1994) focusing on downstroke, and a reverse peel model (Miller and Peskin, 2009), focusing on the clap. Both models assume steady-state flow conditions and circulation averages are representative of the wingbeat. As such, they are simplifications, and caution is necessary in interpreting the results; our goal was to provide initial quantitative estimates to help motivate future research that may employ time-resolved and volumetric techniques for flow measurement (e.g. Hubel et al., 2010; Bomphrey et al., 2012).

We estimate average force produced during the downstroke phase to be 0.74 N – 188% body weight for the average dove weight of 0.39 N. This is consistent with body weight estimates for the downstroke in a dove during steady flight on a level path given that downstroke is 60% of the total wingbeat cycle (Provini et al., 2012).

For the contribution of the clap in the reverse peel model, we incorporated the angle between the wings (50 deg) and induced velocity (2.5 m s^{-1}; Fig. 7). With these values, the reverse peel model indicates the clap phase may produce 0.35 N, or 89% of body weight. The reverse peel model does not include an estimate of force production during the translational phase of the upstroke, and so is likely an underestimate. We estimate the time duration for this average force production to be approximately 10 ms, or 15% of the total wingbeat cycle. In other words, the impulse from downstroke is approximately 0.031 N, while the impulse from upstroke is 0.0035 N.

DISCUSSION

In the two bird species we studied, we observed two distinct aerodynamic patterns, consistent with distinct wing kinematics.

The Journal of Experimental Biology (2015) 218, 2518-2527 doi:10.1242/jeb.116228

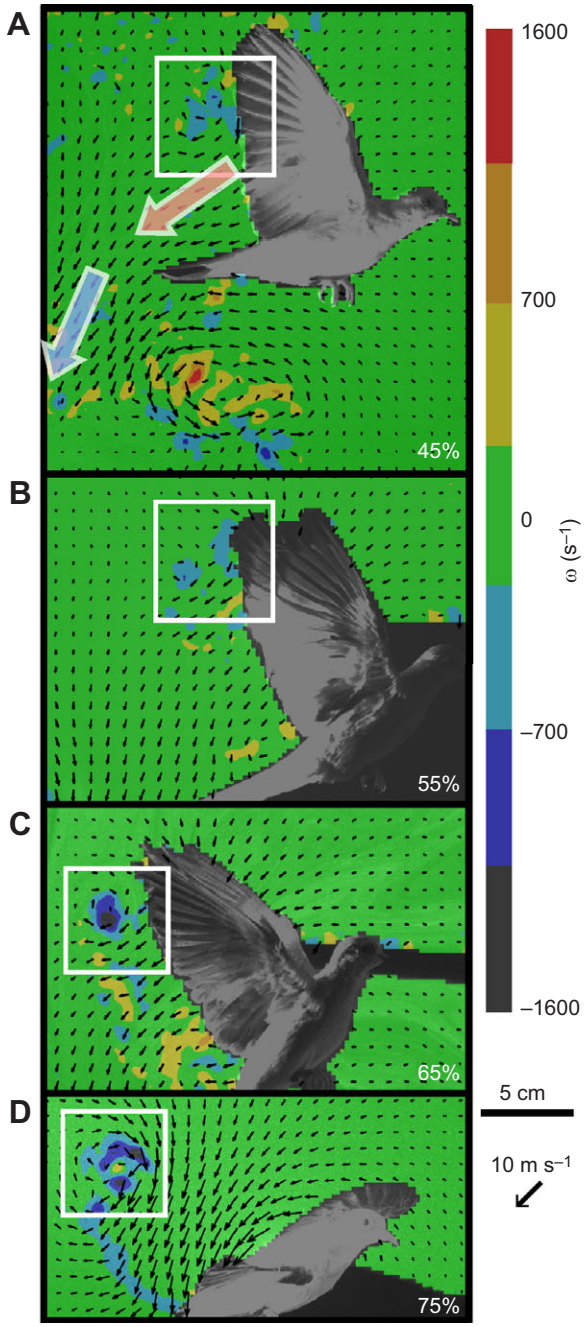

Fig. 4. A sequence of wake visualizations for the diamond dove clap and peel stroke cycle transition. The sequence was assembled using data from two individuals. Vectors in the foreground represent air velocity (m s^{-1}) and colors in the background indicate vorticity (ω, s^{-1}). White boxes indicate the vortex shed during the clap (A) and the downstroke vortex growing during the subsequent peel (B,C) and downstroke (D). Large arrows in A summarize the direction of airflow (blue, downwash from a previous downstroke; red, velocities imparted by the upstroke). The approximate percentage of the wingbeat cycle from kinematics in Figs 2 and 3 is indicated.

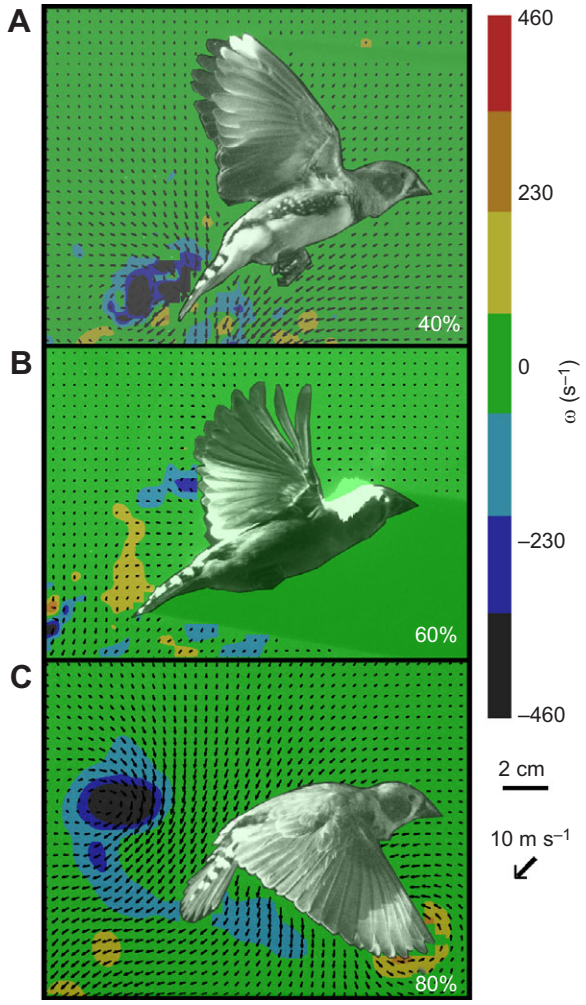

Fig. 5. A sequence of wake visualizations for the zebra finch upstroke to downstroke transition. The sequence was assembled using data from one individual. Vectors in the foreground represent air velocity (m s^{-1}) and colors in the background indicate vorticity (ω, s^{-1}). Note a lack of vorticity at the transition from upstroke to downstroke (A), and a lack of initiation of circulation during the first quarter of downstroke (B), until final levels are reached at the end of downstroke (C). The approximate percentage of the wingbeat cycle from kinematics in Figs 2 and 3 is indicated.

One, the wingtip-reversal upstroke in the dove, produces measurable circulation, evident as a vortex core and induced velocity approximately concurrent with the animal clapping and peeling its wings apart (Figs 4, 7). In contrast, some aerodynamic activity was apparent in streamlines during the flexed-wing upstroke of the zebra finch (Fig. 6B), but this activity was so minimal as to not be manifest in our parasagittal PIV images of the wake from this species (Fig. 5). We found support for our initial hypothesis that the clap and fling style kinematic pattern produces potentially useful aerodynamic forces (estimated at an average of 89% body weight produced during the clap). Further, we found that this capacity to generate aerodynamic force in late upstroke then continues uninterrupted throughout the subsequent downstroke. We found support for our second hypothesis in that the flexed-wing upstroke of the finch produces negligible aerodynamic forces, and as a consequence leads to relatively delayed growth in circulation during the downstroke.

We present α and V_T data for the finch (Fig. 2), but the negligible aerodynamic forces observed suggest that these measures may be irrelevant during the majority of the upstroke, particularly as the wing is kept near the body and so is likely not extended enough to induce momentum to the wake. Although evidence was lacking in our lateral PIV measures, the finch downstroke may be aerodynamically representing a distant-peel condition, wherein the left and right wing do not directly contact, but may be close enough to manifest an aerodynamic benefit similar to the peel

The Journal of Experimental Biology (2015) 218, 2518-2527 doi:10.1242/jeb.116228

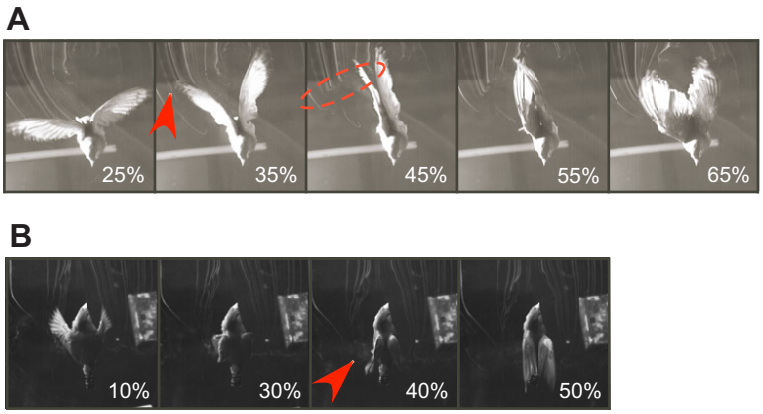

Fig. 6. Smoke-line traces of airflow during flight. (A) In the diamond dove, induced velocity is evident mid-way through the upstroke as a deflection of smoke lines (arrowhead) at 35%, and the disrupted wake visible at 45% (ellipse). (B) In the zebra finch, minimal aerodynamic activity is seen during the upstroke. A small amount of aerodynamic activity is visible at 40% (arrowhead). Approximate percentages of the wingbeat cycle are noted in conjunction with previous figures.

condition (Scholey, 1983). In particular, the peak wingtip velocity in the finch occurs during this phase, and may in fact contribute to the initial creation of circulation. Two passerine species demonstrate clap kinematics at the transition from downstroke to upstroke (Chang et al., 2013), so it is feasible that a similar pattern occurs during the upstroke to downstroke transition. Further work with high-speed, stereo PIV is necessary to explore this hypothesis. Wing inertia may play a crucial role in wing–wing contact (Hedrick et al., 2004); this may serve as an explanation for why short, rounded wing species use a flexed-wing upstroke, and long, pointed wing species typically use a wingtip-reversal upstroke (with the notable exception of the galliformes; Tobalske and Dial, 2000).

The kinematic patterns of the clap and peel during the transition from upstroke to downstroke appear different between insects and birds, likely because of different musculoskeletal arrangements. Birds actively pronate the leading edge of the wing to begin the peel phase, with the trailing edge following. Muscles in the distal wing are active during this phase (Dial, 1992), suggesting muscular control of the distal wing. Insects, however, do not have controlling muscles in their wings, and must rely on forces from indirect muscles deforming the trunk or direct muscles acting at the wing base to separate the two wings (Dudley, 2000). This morphological dissimilarity presents a difference in kinematics. For example, in *E. formosa* during transition from upstroke to downstroke, the clap phase alone constitutes between 20% and 25% of the entire wingbeat cycle (Ellington, 1975). In the dove, this phase is only 2% of the total wingbeat cycle. Further, unlike in theoretical models (Ellington, 1984), the vorticity produced by the clap phase in the dove appeared to be a direct result of shedding circulation created during the upstroke. This is visible in Fig. 6 at 25–45%, and the wake left behind is seen in Fig. 4. In insects, the clap phase expels air from between the left and right wing, similar to a jet (Miller and Peskin, 2009). However, in the dove, circulation created during the upstroke is shed during the clap phase.

The functional contribution of tip-reversal in slow forward flight appears to be as thrust rather than weight support. As the wings are moving caudally, induced velocity in the wake is convected caudally and laterally (supplementary material Movies 2,3). The observed shed vortex is oriented behind the bird, evident in the PIV image (Fig. 4A, red arrow). Shedding of vorticity was likely assisted by the rapid motion of the two wings coming into contact dorsally (Fig. 3, red arrow). In sum, these wing motions and the resulting induction of velocity into the air would likely be beneficial to a bird seeking to move forward. This observation is corroborated by our

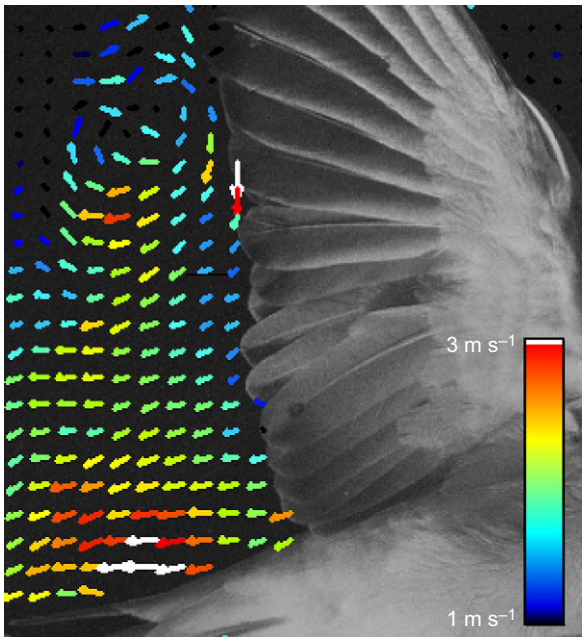

Fig. 7. Induced velocities behind the wing of the diamond dove, caused by motion during upstroke. Velocities behind the wing were created during the upstroke. The scale represents 1–3 m s^{-1}.

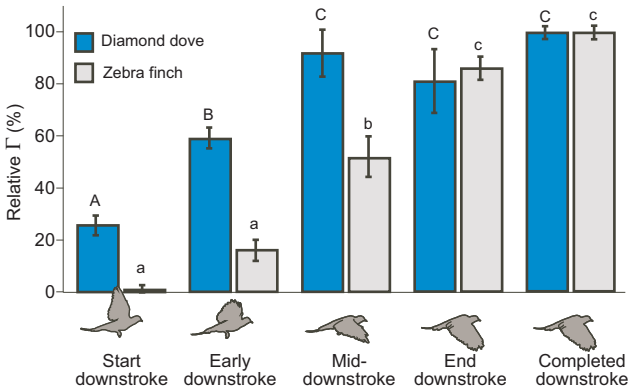

Fig. 8. Circulation during the wingbeat cycle in diamond doves and zebra finches. Circulation (Γ, m^2 s^{-1}) was standardized by dividing by the value of completed downstrokes previously left in the wake. Clap and peel increases circulation starting at the end of upstroke (the 'start downstroke' phase) in the dove, but not the finch. Data are means±s.e. Different letters represent statistically significant differences in mean circulation (P<0.05) within species (uppercase, doves; lowercase, finches). Circulation for each phase was statistically different between species (P<0.01) for all but the end of downstroke phase (P=0.94) and completed downstroke (P=0.97).

The Journal of Experimental Biology (2015) 218, 2518-2527 doi:10.1242/jeb.116228

previous model of the tip-reversal upstroke (Crandell and Tobalske, 2011) and kinematic measurements of whole-body acceleration that are consistent with an aerodynamically active upstroke in pigeons, a species that uses tip-reversal (Ros et al., 2011). Recent measurements in parrotlets (*Forpus coelestis*), a species that exhibits tip-reversal in slow flight, indicates minimal weight support; thrust was not measured (Lentink et al., 2015). This mechanism has the potential to contribute to decelerations during braking, perhaps via interactions with the wake of the previous downstroke. It may additionally contribute to weight support during hovering, although slight kinematic differences likely persist to re-orient flow. The generalities of this mechanism thus merit further study.

Through circulation and vorticity shed via wing–wing interactions, we interpret the clap and peel mechanism supplements circulation produced during downstroke. If this is the case, additional aerodynamic activity may supply additional thrust, potentially providing greater control during slow flight maneuverability (Ros et al., 2011). Further, clap and peel may generate a larger active area swept by the wings, and hence a greater whole-wingbeat span efficiency (Henningsson and Bomphrey, 2011, 2013; Henningsson et al., 2014; Muijres et al., 2011). However, before we can fully understand the details of time-varying force production and span efficiency, it will be essential to obtain better-resolved flow data. Our study will hopefully motivate new tests including time resolution and sampling either the Trefftz plane (Hedenström et al., 2007) or, alternatively, measurements directly on the wing (Muijres et al., 2008; Warrick et al., 2009). Such techniques would offer the opportunity to better estimate instantaneous forces. Further research of the wake flow is necessary using high-speed systems (Hedenström et al., 2009; Henningsson et al., 2011; Hubel et al., 2010) and whole-volume sampling (Bomphrey et al., 2012) to more fully elucidate the three-dimensional and time-varying nature of force production.

Our results add a new example of evolutionary convergence with insects and bats on the use of aerodynamic mechanisms. The clap and peel pattern resulting in a vortex shed in the sagittal plane and induced velocity directed posterior to the animal is consistent with the time-averaged aerodynamic flow pattern created by clap and fling in hawkmoths (Bomphrey et al., 2006). Thus, clap and peel joins leading edge vortices generated during the translational phase of wing movement and rotational circulation during wing reversal (Warrick et al., 2009) as examples of convergence with insects. Bats use a similar wingtip-reversal kinematic pattern during slow flight; however, the aerodynamic activity that has been observed occurs during the translational phase of the hand-wing, producing induced flow behind the animal similar to the flow measurements we have observed before the clap and peel in the dove (Hedenström et al., 2007). As such, bats have likely converged on a similar aerodynamic pattern during upstroke – the generality of the clap and peel in bats, however, remains untested.

Time-varying aerodynamic effects, most notably the leading edge vortex, have been demonstrated in gliding swifts (Videler et al., 2004), a slow flying flycatcher (Muijres et al., 2012a), and modeled in a large, flapping goose (Hubel and Tropea, 2010). Our study extends the understanding of the generality of such convergence across body sizes (and Reynolds numbers), meaning that time-varying aerodynamics are not limited to the smallest of vertebrate fliers (Muijres et al., 2008; Tobalske et al., 2009; Warrick et al., 2009). Diamond doves are 10× the mass of hummingbirds and nectarivorous bats.

The functional contribution of tip-reversal upstroke relative to flexed-wing upstroke begs the question of why it is that not all birds use the tip-reversal and clap and peel mechanisms. Addressing this question will require new insight into the various selective pressures that maintain rounded, low aspect ratio wings in birds. For example, rounded wings are thought to be more useful for avoiding wing damage in cluttered environments. In this context, it is noteworthy that Galliformes with rounded wings use tip-reversal when they are engaged in explosive escape flight after take-off (Tobalske and Dial, 2000). Another explanation was proposed by Vazquez (1992), who suggests there may be a trade-off in function between wrist-bone morphologies allowing a locked-in wing during glide versus those that facilitate the tip-reversal upstroke. In general, though, doves and pigeons glide when engaged in intermittent flight, whereas finches and related small passerines tend to flex their wings and bound (Tobalske, 2001). Further work examining the skeletal function using techniques such as XROMM (Brainerd et al., 2010) is necessary to test the ‘wrist-lock’ hypothesis (Vazquez, 1992).

Conclusions

It has long been recognized that bird species exhibit one of two general upstroke styles during slow flight (Brown, 1948), and here we have demonstrated detailed 3D kinematics and the aerodynamic consequences of these upstroke styles. The zebra finch uses a flexed-wing upstroke, and this upstroke period appears to produce a minimal aerodynamic trace. Diamond doves, with a wingtip-reversal upstroke, exhibit a clap and peel during the upstroke–downstroke transition that generates a shed vortex with measurable induced velocity added to the wake in a way that suggests thrust production that should help the bird progress on a forward path. Further work using time-resolved and volumetric PIV is necessary to refine this initial understanding of the aerodynamic contribution of the upstroke during slow-speed flight in birds.

MATERIALS AND METHODS

Animals and experimental design

Four diamond doves (*G. cuneata*, *Re*=51,000) and four zebra finches (*T. guttata*, *Re*=8500) were trained to fly between two perches positioned 2 m apart within a netted chamber (2×2×2 m) for all but the streamline experiment. For qualifying streamlines, birds flew in the working chamber of a variable-speed wind tunnel (0.6×0.6×0.8 m; see Tobalske et al., 1999, for details of the tunnel design). Information for the morphometrics of each bird is provided in Table 1; Reynolds number was calculated with mean flight velocity during kinematic trials and chord length is reported in Table 1. All procedures were approved by the Institutional Animal Care and Use Committee at the University of Montana.

Kinematics

We recorded wing and body motion using four high-speed video cameras – a Photron SA-3, two PCI 1024 s and a Phantom Miro Ex4, all synchronized using a TTL pulse. Recordings were made at 1000 Hz with a shutter speed of 1/10,000 s. Kinematic analyses of the wings and body during the third wingbeat following take-off were reconstructed in Matlab using a DLT conversion (Hedrick, 2008).

To quantify wing motion, we extracted the global angle of attack (α), global translational wingtip (V_T) and angular velocity (V_A) of the wing in global coordinates for a centroid of the hand-wing in both species (supplementary material Fig. S1). Additionally, to facilitate comparison between species, the wing cycle was divided into relative segments, with 0% and 100% defined as the start of upstroke based on wrist turn-around. The transition between upstroke and downstroke was defined visually at the directional reversal of the wing, and occurred at approximately 28 ms in the dove and 17 ms in the finch. For simplicity, and because we could not obtain time-resolved, whole-volume measures of flow velocity, we did not include induced velocity in our measures of α and V_T.

The Journal of Experimental Biology

The Journal of Experimental Biology (2015) 218, 2518-2527 doi:10.1242/jeb.116228

Several kinematic parameters were calculated for the hand-wing. To compare wing–wing contact, we digitized the wrist, wingtip (10th primary in the dove, 9th primary in the finch), first secondary feather and last secondary feather for both the left and right wing. To compare distances between different points on the wing, we calculated the linear distance between each contralateral point on the corresponding left and right wing.

For additional kinematic parameters, we utilized an average location of the hand-wing. We calculated a hand-wing centroid by averaging the x, y and z position of the wrist, 10th primary (dove) or 9th primary (finch), and the 3rd primary on the left wing. For all parameters presented, we used global coordinates (i.e. not bird-centered). Supplementary material Fig. S1 illustrates each variable described herein. α was calculated by measuring the angle between the hand-wing centroid's velocity vector and a wing chord approximated as a line between the wrist and first secondary feather (approximating a flat wing). V_T (m s^{-1}) was calculated with the direct linear distance between the centroid from frame to frame per unit time (1 ms apart). V_A, or rotational velocity, was calculated as the angle between the hand-wing centroid position vector relative to the shoulder in subsequent frames (1 ms). For all parameters, means and standard deviations across individuals were calculated.

PIV

We used a PIV system (LaVision GmBH, Goettingen, Germany) with DaVis 7.1 software. A dual-cavity pulsed 50 mJ Nd:YAG laser was used to illuminate a 2 mm thick flow field, with planar dimensions spanning a field of approximately 35×25 mm. The laser was oriented behind the flight trajectory, leaving the animal's head in a shadow, so as not to damage its eyes. We seeded the air with particles of olive oil less than 1 µm in diameter, generated at a rate of 7×10^{10} particles s^{-1} using a vaporizer fitted with a Laskin nozzle. Particle illumination was recorded using a 1376×1040 pixel charged-coupled device (CCD) camera placed perpendicular to the illumination field. To calculate particle velocity, we used cross-correlation of paired images with an elapsed time between images of 500 µs. We used a multi-pass filter with an initial interrogation area of 64×64 pixels and a final area of 16×16 pixels with 50% overlap.

We calculated velocity (m s^{-1}), vorticity (ω, s^{-1}) and circulation (Γ, m^2 s^{-1}) as described in Warrick et al. (2009) and Provini et al. (2014). Briefly, we integrated all same-sign ω in a given PIV field within 1.5 chord lengths of peak ω to measure Γ. We considered each negatively signed vortex core deposited in the wake during downstroke to represent the cross-section of an elliptical vortex ring shed from the trailing edge from the wing. In the case of Γ deposited in the wake due to upstroke, we used a visual cut-off of streamlines to quantify the presence of Γ (see fig. 3 in Provini et al., 2012). This anomalous vorticity was considered to be created from the motion of the upstroke during the wing-tip reversal upstroke and is likely the result of vorticity shed from the wingtip. Average free-stream background vorticity was measured at 0.006±0.008 s^{-1}, 1.5% of average peak vorticity measured in the wake for the birds. Thus, we applied no masking. Added mass of the vortex wake was not calculated, as we lacked adequate time resolution to measure displacement of shed vortices (Dabiri, 2005). It has been previously shown in chukar partridge (*Alectoris chukar*) that birds generate negligible aerodynamic added mass (Tobalske and Dial, 2007).

We sampled the near-wake of the birds in a parasagittal plane (±1 cm from sagittal plane). Samples were taken at 5 Hz, and were recorded during the initial 3rd to 5th wingbeat after takeoff from a perch, at body velocities of approximately 3 m s^{-1} for the doves and 1.5 m s^{-1} for the finches. To quantify growth in Γ with respect to time, we divided the wingbeat into four phases: (1) transition from upstroke to downstroke (dove N=19, finch N=9; approximately 40–50% of the entire wingbeat cycle; Figs 2, 3); (2) first quarter of downstroke (dove N=30, finch N=16; approximately 50–63% of the wingbeat cycle); (3) second quarter of downstroke (dove N=20, finch N=13; approximately 63–75% of the wingbeat cycle); and (4) third and fourth quarters of downstroke (dove N=14, finch N=21; approximately 75–100% of the wingbeat cycle) based on wingtip elevation and depression relative to the bird. We measured previously shed downstroke Γ left in the wake for comparison with the most recently completed wingbeat (dove N=124, finch N=82). We tested for differences in the time course of circulation between birds using a one-way ANOVA, with individual as a factor, and found no differences in mean downstroke force production among individuals (for doves: $0.76<P<0.99$, for finches: $0.33<P<0.98$); thus, all birds were combined for final analyses. Herein, we report means±s.d. To compare phases within species, we used a one-way ANOVA with phase as a factor, followed by a Tukey *post hoc* test to determine significant differences between phases. To compare the percentage circulation during each phase between species, we used a Student's t-test.

Time-resolved flow

To more fully observe flow characteristics with respect to time and volume, we employed a classic smoke streamline study (Barlow et al., 1999; Ellington et al., 1996). We installed a nichrome wire (60 gauge) horizontally across the front of the working section of a variable speed wind tunnel (Tobalske et al., 1999). This wire was connected to a 15 V power supply. We seeded the wire with mineral oil droplets approximately 0.5 cm apart. When current was applied to the wire, it produced heat, and the droplets burnt to create streamlines. For these experiments, air velocity in the tunnel was 0.95±0.05 m s^{-1}. One dove and one finch were flown within the tunnel, and the flight and smoke flow were recorded from a dorsal view using a Photron PCI 1024 high-speed camera recording at 1000 frames s^{-1}, with a shutter speed of 1/5000 s.

Force estimates

To gain an approximation of body weight support provided by the aerodynamic mechanisms we observed, we utilized two models. To estimate net force during the downstroke, we used a momentum jet model, as described by Vogel (1994):

$$F = \rho\Gamma A/T. \quad (1)$$

We used this calculation for each quarter of the downstroke divided equally by time (T=9.25 ms), with corresponding measures of Γ (see Fig. 8) and swept wing area A, for each quarter, where air density ρ=1.07 kg m^{-3} in Missoula, MT, USA. We then averaged the momentum jet model calculated for each section, for a net force estimate.

As a rough estimate of potential force production of the clap phase, we elected to use the reverse peel model (Miller and Peskin, 2009). This estimation was only possible for the dove, as the finch did not have a kinematic pattern close to a clap and peel, and so we could not estimate the angle between the two wings. The reverse peel is modeled as:

$$F = \rho\beta c u^2, \quad (2)$$

where β is the estimated angle between the two wings for the last 10 ms of the clap (approximately 50 deg in the dove), c is the wing chord and u is the average airspeed resulting from the clap (Fig. 7).

Acknowledgements

We would like to thank Heather Labbe for assistance with data collection, and Andy Biewener, Tom Brekke, Doug Emlen, Art Woods, the UMT Morphology Group and anonymous reviewers for valuable insight.

Competing interests

The authors declare no competing or financial interests.

Author contributions

Both authors were involved in the research design, interpretation of findings and preparation of the manuscript. K.E.C. additionally performed the experiments and analyzed the data.

Funding

K.E.C. was funded by a NASA-Montana Space Grant Consortium (MSGC) Graduate Research Fellowship and this work was also funded by National Science Foundation Grants IOS-0923606 and IOS-0919799.

Supplementary material

Supplementary material available online at
http://jeb.biologists.org/lookup/suppl/doi:10.1242/jeb.116228/-/DC1

References

Barlow, J., Rae, W. and Pope, A. (1999). *Low-Speed Wind Tunnel Testing*. Canada: John Wiley & Sons.

Bennett, L. (1977). Clap and fling aerodynamics - experimental evaluation. *J. Exp. Biol.* **69**, 261-272.

Berg, A. M. and Biewener, A. A. (2010). Wing and body kinematics of takeoff and landing flight in the pigeon (*Columba livia*). *J. Exp. Biol.* **213**, 1651-1658.

Bomphrey, R. J., Lawson, N. J., Taylor, G. K. and Thomas, A. L. R. (2006). Application of digital particle image velocimetry to insect aerodynamics: measurement of the leading-edge vortex and near wake of a Hawkmoth. *Exp. Fluids* **40**, 546-554.

Bomphrey, R. J., Henningsson, P., Michaelis, D. and Hollis, D. (2012). Tomographic particle image velocimetry of desert locust wakes: instantaneous volumes combine to reveal hidden vortex elements and rapid wake deformation. *J. R. Soc. Interface.* **9**, 3378-3386.

Brainerd, E. L., Baier, D. B., Gatesy, S. M., Hedrick, T. L., Metzger, K. A., Gilbert, S. L. and Crisco, J. J. (2010). X-Ray reconstruction of moving morphology (XROMM): precision, accuracy, and applications in comparative biomechanics research. *J. Exp. Zool.* **313A**, 262-279.

Brown, R. H. J. (1948). The flight of birds - the flapping cycle of the pigeon. *J. Exp. Biol.* **25**, 322-333.

Brown, R. H. J. (1953). The flight of birds 2. Wing function in relation to flight speed. *J. Exp. Biol.* **30**, 90-103.

Brown, R. H. J. (1963). The flight of birds. *Biol. Rev. Camb. Philos. Soc.* **38**, 460-489.

Chang, Y.-H., Ting, S.-C., Su, J.-Y., Soong, C.-Y. and Yang, J.-T. (2013). Ventral-clap modes of hovering passerines. *Phys. Rev. E* **87**, 022707.

Corning, W. R. and Biewener, A. A. (1998). *In vivo* strains in pigeon flight feather shafts: implications for structural design. *J. Exp. Biol.* **201**, 3057-3066.

Crandell, K. E. and Tobalske, B. W. (2011). Aerodynamics of tip-reversal upstroke in a revolving pigeon wing. *J. Exp. Biol.* **214**, 1867-1873.

Dabiri, J. O. (2005). On the estimation of swimming and flying forces from wake measurements. *J. Exp. Biol.* **208**, 3519-3532.

Dial, K. P. (1992). Activity patterns of the wing muscles of the pigeon (*Columba livia*) during different modes of flight. *J. Exp. Zool.* **262**, 357-373.

Dudley, R. (2000). *The Biomechanics of Insect Flight*. NJ, USA: Princeton University Press.

Earls, K. D. (2000). Kinematics and mechanics of ground take-off in the starling *Sturnis vulgaris* and the quail *Coturnix coturnix*. *J. Exp. Biol.* **203**, 725-739.

Ellington, C. (1975). Non-steady state aerodynamics of the flight of *Encarsia formosa*. In *Swimming and Flying in Nature* (ed. T. W.-T. Wu, C. J. Brokaw and C. Brennen). New York, NY, USA: Plenum Press.

Ellington, C. P. (1984). The aerodynamics of hovering insect flight. IV. Aerodynamic mechanisms. *Philos. Trans. R. Soc. Lond. B Biol. Sci.* **305**, 79-113.

Ellington, C. P., Van Den Berg, C., Willmott, A. P. and Thomas, A. L. (1996). Leading-edge vortices in insect flight. *Nature* **384**, 626-630.

Hedenström, A., Rosén, M. and Spedding, G. R. (2006). Vortex wakes generated by robins *Erithacus rubecula* during free flight in a wind tunnel. *J. R. Soc. Interface* **3**, 263-276.

Hedenström, A., Johansson, L. C., Wolf, M., von Busse, R., Winter, Y. and Spedding, G. R. (2007). Bat flight generates complex aerodynamic tracks. *Science* **316**, 894-897.

Hedenström, A., Muijres, F. T., von Busse, R., Johansson, L. C., Winter, Y. and Spedding, G. R. (2009). High-speed stereo DPIV measurement of wakes of two bat species flying freely in a wind tunnel. *Exp. Fluids* **46**, 923-932.

Hedrick, T. L. (2008). Software techniques for two- and three-dimensional kinematic measurements of biological and biomimetic systems. *Bioinspir. Biomim.* **3**, 034001.

Hedrick, T. L., Usherwood, J. R. and Biewener, A. A. (2004). Wing inertia and whole-body acceleration: an analysis of instantaneous aerodynamic force production in cockatiels (Nymphicus hollandicus) flying across a range of speeds. *J. Exp. Biol.* **207**, 1689-1702.

Henningsson, P. and Bomphrey, R. J. (2011). Time-varying span efficiency through the wingbeat of desert locusts. *J. R. Soc. Interface*, rsif20110749.

Henningsson, P. and Bomphrey, R. J. (2013). Span efficiency in hawkmoths. *J. R. Soc. Interface* **10**, 20130099.

Henningsson, P., Muijres, F. T. and Hedenstrom, A. (2011). Time-resolved vortex wake of a common swift flying over a range of flight speeds. *J. R. Soc. Interface* **8**, 807-816.

Henningsson, P., Hedenström, A. and Bomphrey, R. J. (2014). Efficiency of lift production in flapping and gliding flight of swifts. *PLoS ONE* **9**, e90170.

Hubel, T. Y. and Tropea, C. (2010). The importance of leading edge vortices under simplified flapping flight conditions at the size scale of birds. *J. Exp. Biol.* **213**, 1930-1939.

Hubel, T. Y., Riskin, D. K., Swartz, S. M. and Breuer, K. S. (2010). Wake structure and wing kinematics: the flight of the lesser dog-faced fruit bat, Cynopterus brachyotis. *J. Exp. Biol.* **213**, 3427-3440.

Lehmann, F.-O., Sane, S. P. and Dickinson, M. (2005). The aerodynamic effects of wing-wing interaction in flapping insect wings. *J. Exp. Biol.* **208**, 3075-3092.

Lentink, D., Haselsteiner, A. F. and Ingersoll, R. (2015). In vivo recording of aerodynamic force with an aerodynamic force platform: from drones to birds. *J. R. Soc. Interface* **12**, 20141283.

Lorenz, K. (1933). Beobachtetes über das Fliegen der Vögel und über die Beziehungen der Flügel- und Steuerform zur Art des Fluges. *J. Ornithol.* **81**, 107-236.

Marey, E. (1890). *Locomotion Dans L'air*. In *Le Vol Des Oiseaux*. Paris, France: Le Mouvement.

Maxworthy, T. (1979). Experiments on the Weis-Fogh mechanism of lift generation by insects in hovering flight. Part 1. Dynamics of the 'fling'. *J. Fluid Mech.* **93**, 47.

Miller, L. A. and Peskin, C. S. (2009). Flexible clap and fling in tiny insect flight. *J. Exp. Biol.* **212**, 3076-3090.

Muijres, F. T., Johansson, L. C., Barfield, R., Wolf, M., Spedding, G. R. and Hedenstrom, A. (2008). Leading-edge vortex improves lift in slow-flying bats. *Science* **319**, 1250-1253.

Muijres, F. T., Spedding, G. R., Winter, Y. and Hedenström, A. (2011). Actuator disk model and span efficiency of flapping flight in bats based on time-resolved PIV measurements. *Exp. Fluids* **51**, 511-525.

Muijres, F. T., Bowlin, M. S., Johansson, L. C. and Hedenstrom, A. (2012a). Vortex wake, downwash distribution, aerodynamic performance and wingbeat kinematics in slow-flying pied flycatchers. *J. R. Soc. Interface* **9**, 292-303.

Muijres, F. T., Johansson, L. C., Bowlin, M. S., Winter, Y. and Hedenström, A. (2012b). Comparing aerodynamic efficiency in birds and bats suggests better flight performance in birds. *PLoS ONE* **7**, e37335.

Muijres, F. T., Johansson, L. C. and Hedenström, A. (2012c). Leading edge vortex in a slow-flying passerine. *Biol. Lett.*, rsbl20120130.

Pournazeri, S., Segre, P. S., Princevac, M. and Altshuler, D. L. (2013). Hummingbirds generate bilateral vortex loops during hovering: evidence from flow visualization. *Exp. Fluids* **54**, 1439.

Provini, P., Tobalske, B. W., Crandell, K. E. and Abourachid, A. (2012). Transition from leg to wing forces during take-off in birds. *J. Exp. Biol.* **215**, 4115-4124.

Provini, P., Tobalske, B. W., Crandell, K. E. and Abourachid, A. (2014). Transition from wing to leg forces during landing in birds. *J. Exp. Biol.* **217**, 2659-2666.

Ros, I. G., Bassman, L. C., Badger, M. A., Pierson, A. N. and Biewener, A. A. (2011). Pigeons steer like helicopters and generate down- and upstroke lift during low speed turns. *Proc. Natl. Acad. Sci. USA* **108**, 19990-19995.

Sane, S. P. (2003). The aerodynamics of insect flight. *J. Exp. Biol.* **206**, 4191-4208.

Scholey, K. D. (1983). Developments in vertebrate flight: climbing and gliding of mammals and reptiles, and the flapping flight of birds. PhD thesis, University of Bristol, UK.

Simpson, S. F. (1983). The flight mechanism of the pigeon *Columbia livia* during take-off. *J. Zool.* **200**, 435-443.

Spedding, G. R. and Hedenström, A. (2009). PIV-based investigations of animal flight. *Exp. Fluids* **46**, 749-763.

Spedding, G. R., Hedenström, A. and Rosén, M. (2003a). Quantitative studies of the wakes of freely flying birds in a low-turbulence wind tunnel. *Exp. Fluids* **34**, 291-303.

Spedding, G. R., Rosén, M. and Hedenström, A. (2003b). A family of vortex wakes generated by a thrush nightingale in free flight in a wind tunnel over its entire natural range of flight speeds. *J. Exp. Biol.* **206**, 2313-2344.

Tobalske, B. W. and Dial, K. P. (1996). Flight kinematics of black-billed magpies and pigeons over a wide range of speeds. *J. Exp. Biol.* **199**, 263-280.

Tobalske, B. W. (2001). Morphology, velocity, and intermittent flight in birds. *Amer. Zool.* **41**, 177-187.

Tobalske, B. W. (2007). Biomechanics of bird flight. *J. Exp. Biol.* **210**, 3135-3146.

Tobalske, B. W. and Dial, K. P. (2000). Effects of body size on take-off flight performance in the Phasianidae (Aves). *J. Exp. Biol.* **203**, 3319-3332.

Tobalske, B. W. and Dial, K. P. (2007). Aerodynamics of wing-assisted incline running in birds. *J. Exp. Biol.* **210**, 1742-1751.

Tobalske, B. W., Peacock, W. L. and Dial, K. P. (1999). Kinematics of flap-bounding flight in the zebra finch over a wide range of speeds. *J. Exp. Biol.* **202**, 1725-1739.

Tobalske, B. W., Hedrick, T. L., Dial, K. P. and Biewener, A. A. (2003). Comparative power curves in bird flight. *Nature* **421**, 363-366.

Tobalske, B. W., Hearn, J. W. D. and Warrick, D. R. (2009). Aerodynamics of intermittent bounds in flying birds. *Exp. Fluids* **46**, 963-973.

Vazquez, R. J. (1992). Functional osteology of the avian wrist and the evolution of flapping flight. *J. Morphol.* **211**, 259-268.

Videler, J. J., Stamhuis, E. J. and Povel, G. D. E. (2004). Leading-edge vortex lifts swifts. *Science* **306**, 1960-1962.
Vogel, S. (1967). Flight in drosophila 3. Aerodynamic characteristics of fly wings and wing models. *J. Exp. Biol.* **46**, 431.
Vogel, S. (1994). *Life in Moving Fluids: The Physical Biology of Flow*. Princeton, NJ: Princeton University Press.
Warrick, D. R., Tobalske, B. W. and Powers, D. R. (2005). Aerodynamics of the hovering hummingbird. *Nature* **435**, 1094-1097.
Warrick, D. R., Tobalske, B. W. and Powers, D. R. (2009). Lift production in the hovering hummingbird. *Proc. R. Soc. B Biol. Sci.* **276**, 3747-3752.
Weis-Fogh, T. (1973). Quick estimates of flight fitness in hovering animals, including novel mechanisms for lift production. *J. Exp. Biol.* **59**, 169-230.

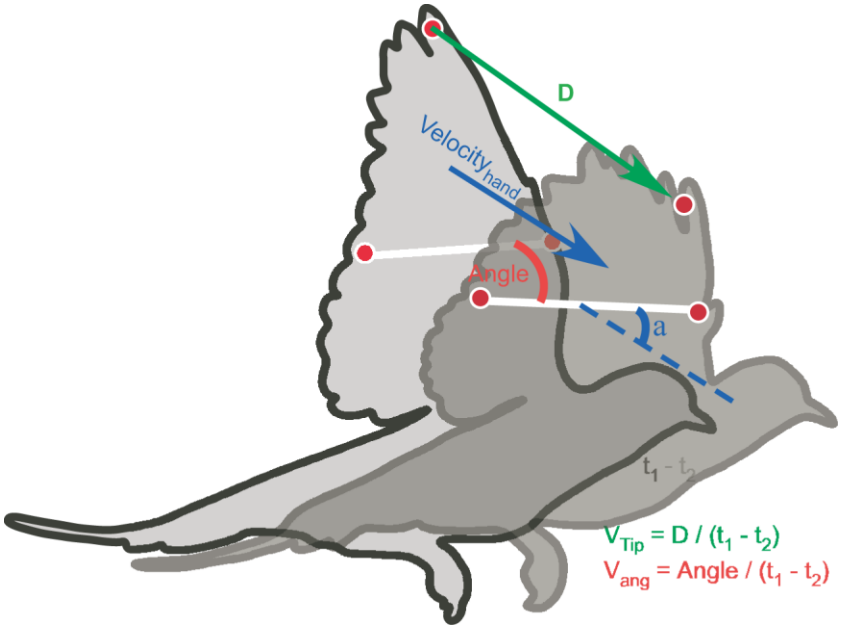

Fig. S1. Descriptors of variables measured in kinematic analyses. Red dots represent markers drawn on the bird with sharpie at the wrist, tip of the primary feather, and the first secondary feather. V_{tip} and V_{ang} required the use of two time intervals (represented as t_1, light gray silhouette; and t_2, dark gray silhouette).

Movie 1. Streamlines reveal smoke entrained on the distal primary feathers of the finch during upstroke. However, this minor induced momentum was not visible in PIV images.

Movie 2. Streamlines reveal entrained air during the wingtip-reversal in the diamond dove. During mid-upstroke, streamlines are disrupted by the wing.

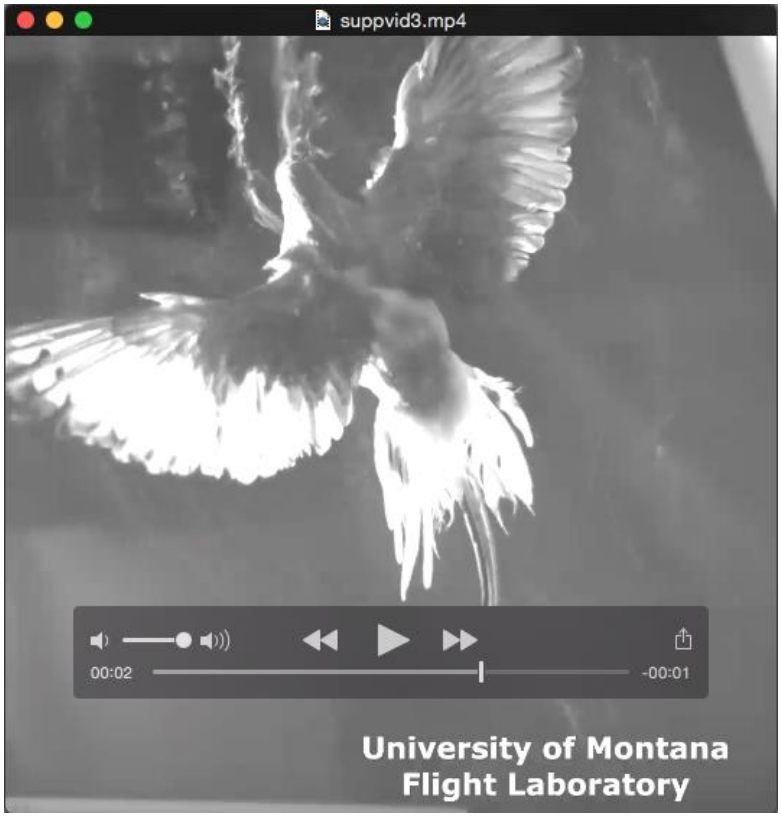

Movie 3. Streamlines during the transition from upstroke to downstroke in the diamond dove. Induced momentum to the wake is visible behind the bird following the "clap" (dorsal contact between the left and right wing).